

Monolithic integration of ultraviolet microdisk lasers into photonic circuits in a III-nitride-on-silicon platform

FARSANE TABATABA-VAKILI^{1,2}, BLANDINE ALLOING³, BENJAMIN DAMILANO³, HASSEN SOUISSI⁴, CHRISTELLE BRIMONT⁴, LAETITIA DOYENNETTE⁴, THIERRY GUILLET⁴, XAVIER CHECOURY¹, MOUSTAFA EL KURDI¹, SÉBASTIEN CHENOT³, ERIC FRAYSSINET³, JEAN-YVES DUBOZ³, FABRICE SEMOND³, BRUNO GAYRAL², AND PHILIPPE BOUCAUD^{3,*}

¹ Université Paris-Saclay, CNRS, C2N, 91120, Palaiseau, France.

² Univ. Grenoble Alpes, CEA, IRIG-Pheliqs, 38000 Grenoble, France.

³ Université Côte d'Azur, CNRS, CRHEA, 06560 Valbonne, France.

⁴ L2C, Université de Montpellier, CNRS, 34095 Montpellier, France.

* Corresponding author: Philippe.Boucaud@crhea.cnrs.fr

Compiled July 30, 2020

Ultraviolet microdisk lasers are integrated monolithically into photonic circuits using a III-nitride on silicon platform with gallium nitride (GaN) as the main waveguiding layer. The photonic circuits consist of a microdisk and a pulley waveguide terminated by out-coupling gratings. We measure quality factors up to 3500 under continuous-wave excitation. Lasing is observed from 374 nm to 399 nm under pulsed excitation, achieving low threshold energies of 0.14 mJ/cm² per pulse (threshold peak powers of 35 kW/cm²). A large peak to background dynamic of around 200 is observed at the out-coupling grating for small gaps of 50 nm between the disk and waveguide. These devices operate at the limit of what can be achieved with GaN in terms of operation wavelength. © 2020 Optical Society of America

<http://dx.doi.org/10.1364/ao.XX.XXXXXX>

In recent years, there has been a significant interest in ultraviolet (UV) emitters, such as light emitting diodes (LEDs) and optically pumped lasers for a variety of applications including germicidal sterilization and gas sensing [1, 2]. The material system of choice for active devices in the UV spectrum is III-nitride, due to its band gap tunability from the UV-C to the visible spectrum.

III-nitride microcavity photonics is a very active field of research [3]. Individual microlasers in the UV spectral range have been realized under pulsed optical pumping [4–6] and electrical injection [7]. Photonic circuits in the UV have also recently gained popularity with potential applications including atomic clocks or precision metrology [8]. Several passive circuits have been demonstrated using aluminum nitride (AlN) [9–12] or aluminum oxide (Al₂O₃) [13]. A simple active circuit using aluminum gallium nitride (AlGaN) LEDs has also recently been demonstrated [14]. However, no demonstrations of active photonic circuits containing microlasers in the UV have been

reported, while this would constitute an important step for the development of next generation photonic circuits.

Meanwhile, there have been several reports of optically pumped active microlaser photonic circuits in the blue using III-nitrides [15–17], as well as efforts to combine microrings under electrical injection with photonic circuits [18].

In this Letter, we report on the demonstration of active microlaser photonic circuits in the UV consisting of a microdisk, a pulley waveguide, and out-coupling gratings terminating the waveguide.

The investigated sample was grown by metal organic chemical vapor deposition (MOCVD) on silicon (111). First, a 220 nm AlN buffer layer was grown, followed by 300 nm of GaN. Then the active region containing 5 pairs of 2 nm In_xGa_{1-x}N / 9 nm GaN quantum wells (QWs) (nominal indium composition $x = 0.1$) was grown, followed by a 20 nm GaN cap layer. The total thickness is around 600 nm.

We fabricated microdisk photonic circuits using a process similar to the one described in Refs. [15, 16]. An SiO₂ hard mask, e-beam lithography using UV5 resist, and inductively coupled plasma (ICP) etching with CH₂F₂ and CF₄ gases for the SiO₂ and Cl₂ and BCl₃ gases for the III-nitrides were employed. The process consisted of two levels of lithography and etching. First, the microdisk, waveguide and grating couplers were defined, using proximity effect correction at the gap and a higher e-beam dose for the grating coupler. After the ICP etch, we performed a chemical treatment with AZ400K developer at 40°C to smooth the side-walls. In the second level, we opened an area containing the waveguide to etch away the QWs in order to avoid re-absorption of the emission. Finally, the silicon was underetched using XeF₂ gas to provide for vertical confinement by refractive index contrast to air. We fabricated devices with 3 μm diameter disks and waveguides with an angle of 180° around the disk with nominally 125 nm width in the proximity of the disk and 500 nm width away from the disk. The distance from the center of the microdisk to the end of the waveguide is 50 μm. The grating couplers have a period of 200 nm. The

gap between the disk and the waveguide is varied between 40 and 100 nm. These devices are particularly challenging to fabricate due to the fairly long suspension length of the waveguide with the 180° bend. For larger microdisks we observe cracking of the nanotethers that hold the waveguide, which then falls. For suspension lengths smaller than 12 μm the devices are stable. Thus, our devices are at the fabrication limit of suspended photonic circuits in this platform. The reason for using a 180° waveguide bend is the increase in coupling length that allows to have efficient coupling at larger gaps. Using finite-difference time-domain (FDTD) simulations we estimate that the critical coupling gap is 20 nm larger than for a 90° angle (60 nm instead of 40 nm) corresponding to the maximum coupling.

Fig. 1 (a) shows an optical microscope image of a fabricated device, clearly showing the underetched areas as well as the waveguide etch through color-contrast. Fig. 1 (b) shows a scanning electron microscope (SEM) image of a device, also indicating the underetch and clearly showing the nanotethers that hold the waveguide. Zoom-ins of the microdisk, the gap and the grating coupler are shown in Figs. 1 (c)-(e). In Fig. 1 (d) we can see the roughness of our very thin waveguides (nominally 125 nm), which is visible due to the large zoom.

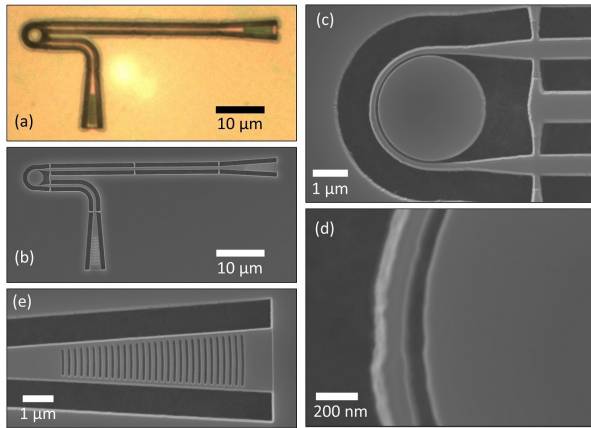


Fig. 1. (a) Optical microscope image and (b) SEM image of a photonic circuit. Zoom-ins of (c) the microdisk, (d) the coupling region, and (e) the grating coupler.

We employ a standard μ-photoluminescence (μ-PL) setup with a continuous-wave (CW) laser emitting at 355 nm and a 20x microscope objective that is used to pump the device and to collect the emission that is then measured by a spectrometer and a charge-coupled device (CCD). A map of the CCD allows to differentiate between the emission from the disk and from the grating by integrating over different areas. We pump the microdisks at room temperature (RT) in order to determine the loaded Q factors of our devices. The bottom part of Fig. 2 shows a CW spectrum measured from the top at the out-coupling grating for a device with 100 nm gap. Many modes are visible and their identification is difficult. We observe first-order modes with an FSR of 4 nm at 407.7 nm, 411.8 nm, and 415.4 nm with Q_{load} in the range of 1400 to 1800, which are limited by QW absorption. The maximum Q_{load} for the 100 nm gap is 3500 at 419.7 nm (potentially the next first-order mode), which is shown in the inset in Fig. 2. We note that under low power density CW excitation the QW emission is centered at around 407 nm. The modes are not or barely visible above the microdisk under CW excitation in our top-collection setup, as whispering gallery

modes (WGMs) radiate preferentially in-plane. Based on the Q_{load} of the 100 nm gap device, we assume that the intrinsic Q factor Q_{int} is 3500, which is in the same order of magnitude as for our previously investigated microdisks [5, 16, 19]. The Q_{load} at 380 nm will certainly be lower due to the GaN absorption. Q_{int} might be limited by side-wall roughness or surface absorption [20].

We can estimate the effective propagation losses of the microdisk using [21]

$$\alpha_{disk} = \frac{\lambda_0}{Q_{int} \cdot FSR \cdot r'} \quad (1)$$

with λ_0 the resonance wavelength, FSR the free spectral range, and r the radius of the disk. We obtain $\alpha = 0.08$ dB/μm when extrapolating at $\lambda_0 = 380$ nm, $FSR = 4$ nm, $Q_{int} = 3500$, and $r = 1.5$ μm, which is two orders of magnitude larger than reported by Liu et al. for AlN microrings at 390 nm [12] and in the same order of magnitude as reported by Stegmaier et al. for polycrystalline AlN waveguides at 400 nm [9]. When comparing with Ref. [12], we need to consider several factors. Firstly, the different waveguiding material, GaN vs. AlN: GaN will have higher losses due to larger material absorption at 380 nm, an absorption of 100 cm⁻¹ would result in a Q_{abs} of 4200. Secondly, the much higher radiation loss due to strong bending of a small microdisk ($r = 1.5$ μm) as compared to a large microring ($r = 30$ μm) [22]. Thirdly, the different refractive index contrasts between waveguide and cladding (air vs. SiO₂/Al₂O₃): a smaller index contrast results in significantly lower scattering loss due to roughness. Lastly, the growth substrate, Si vs sapphire: a smaller dislocation density, which can be more easily achieved on sapphire, can induce lower internal losses. Furthermore, we employ much smaller gaps between the resonator and the waveguide than Liu et al., which renders our process more complex, but leads to better cavity to waveguide coupling.

In analogy to Ref. [12], we calculate $H_{z,s}^2 / (\int H_z^2 dx dz)$, where $H_{z,s}$ is the the maximum field at the side-wall of the disk and the integral is taken over the x-z cross-section, where z is the out-of-plane direction, using FDTD. For our microdisk, we obtain 2.3 μm⁻², which is an order of magnitude larger than the value obtained by Liu et al. for wide microrings [12]. The higher field at the interface can be explained by the larger curvature of a small disk compared to a large ring and results in larger side-wall losses, explaining in part the lower Q factor we observe.

Lasng is observed at RT under pulsed optical conditions using a laser at 355 nm with 7 kHz repetition rate and 4 ns pulse width. Fig. 2 shows pulsed spectra at peak powers of 34 kW/cm² ($0.9E_{th}$) and 101 kW/cm² ($2.7E_{th}$) measured at the out-coupling grating for a device with 100 nm gap. A strong blue-shift of around 25 nm is observed with increasing excitation power as we go from CW to pulsed excitation far above threshold. The blue-shift can be explained both by quantum confined Stark effect screening at large carrier density and by state-filling of localized states of the InGaN QWs. A smaller blue-shift was observed in our previous samples, as they were grown by molecular beam epitaxy (MBE) where less localization is observed [16]. Furthermore, it is very likely that excited states in the QWs are lasing. Considering the e1 (electron ground state) to hh1 (heavy hole ground state) transition at 3.05 eV or 407 nm, the center emission wavelength under low excitation CW pumping, an Indium composition of 13.5% in the QWs is deduced from 6 band **k.p** simulations without considering carrier interactions. This transition has an oscillator strength of 0.34. The QWs are

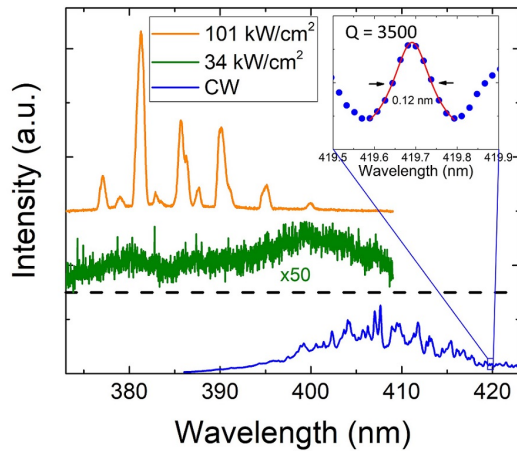


Fig. 2. Spectra below and above threshold taken at the out-coupling grating for devices with 100 nm gap. Bottom: Low-excitation power density CW spectrum below threshold. The inset shows the maximum Q factor of 3500 at the low energy side of the spectrum at 419.7 nm. Top: Pulsed spectra below and above threshold. The spectra are displaced along the y-axis and the CW spectrum has a different y-scale.

very asymmetric, which makes the cross-transitions ($e2\text{-hh}1$ and $e1\text{-hh}2$, where 2 denotes the first excited state) very intense. The oscillator strength of the $e2\text{-hh}1$ transition at 3.31 eV or 375 nm is 0.23. For the $e1\text{-hh}2$ transition at 3.13 eV or 396 nm we get an oscillator strength of 0.12. The emission thus encompasses the entire lasing spectral range of our devices.

The lasing modes are rather broad. The mode at 381.2 nm at $2.7E_{th}$ has a full-width at half maximum (FWHM) of 1 nm. Generally under pulsed pumping, linewidths are broader than under CW pumping since the carrier density changes strongly in the microlaser during one pulse (here 4 ns). We do not observe linewidth narrowing near the threshold, since the modes are not visible below threshold due to the limited signal to noise ratio under these low duty-cycle conditions.

Figs. 3 (a) and (c) show pulse energy dependent spectra measured above the microdisk for devices with 50 nm and 90 nm gaps, respectively. Spectra measured on the same devices but at the out-coupling grating are depicted in Figs. 3 (b) and (d). Lasing modes are observed from 374 nm to 399 nm. The lowest threshold energy of $0.14 \text{ mJ}/\text{cm}^2$ per pulse or threshold peak power of $35 \text{ kW}/\text{cm}^2$ is observed for the 80 nm gap (not shown). The calculated overlap of the vertical TE_0 mode with the QWs (excluding the barriers) is 1.0%. This value could be increased by using cladding layers, but those would result in a much thicker structure that makes suspended photonic circuits more difficult to fabricate.

The first-order radial WGMs are visible for both 50 nm and 90 nm gaps (Fig. 3) with a spacing of 3.6 to 4.6 nm and azimuthal mode orders of $m = 60$ at 374 nm to $m = 54$ at 399 nm, as determined by FDTD simulations. First one and then several first order modes lase, followed by other modes of higher order, which are especially visible at high energy for the larger gaps (Figs. 2 and 3 (c,d)). We observe a very large dynamic of the peak to background emission of around 200 at $3E_{th}$ for the 50 nm gap device at the grating coupler, with only a factor 10 observed directly at the disk. The improvement of this dynamic with increased coupling is due to the fact that the WGMs radiate

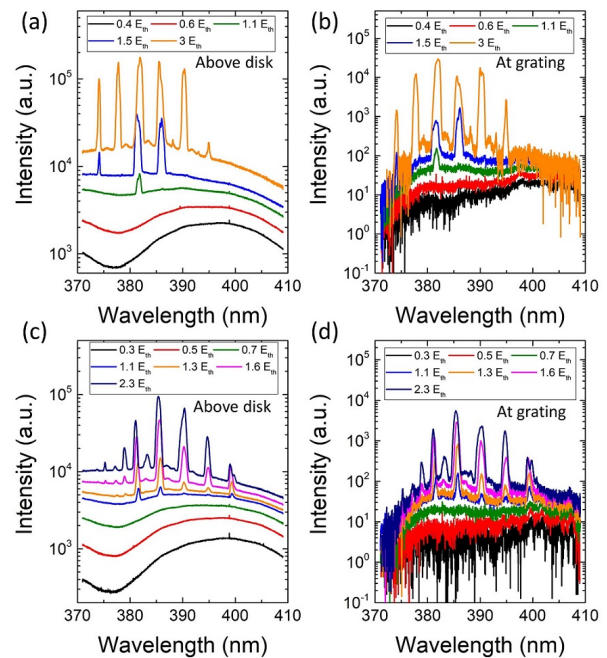


Fig. 3. Energy dependent pulsed optical pumping spectra of measured (a,c) above the disk and (c,d) at the grating coupler for devices with (a,b) a 50 nm gap and (c,d) an 90 nm gap. The thresholds are $0.18 \text{ mJ}/\text{cm}^2$ per pulse for the 50 nm gap and $0.15 \text{ mJ}/\text{cm}^2$ per pulse for the 90 nm gap.

preferentially in-plane, while the spontaneous QW emission radiates mainly out-of-plane. In FDTD transmission simulations we obtain a maximum coupling of 70% for a gap of 60 nm.

The threshold peak powers, reported here, for pulsed III-nitride microdisk lasers are lower than what we have found in literature. Simeonov et al. reported $166 \text{ kW}/\text{cm}^2$ at 409 nm [23] and Zhu et al. $180 \text{ kW}/\text{cm}^2$ at 380 nm [6]. We reported lasing thresholds of $300 \text{ kW}/\text{cm}^2$ for microdisk photonic circuits operating at 420 nm [16]. The threshold reduction of one order of magnitude for our samples is primarily due to a change in growth method from MBE to MOCVD for our QWs. MBE grown QWs have a lower radiative efficiency due to a higher concentration of point defects caused by the lower growth temperature [24]. We can compare our thresholds to pulsed electrically injected lasing reported by Wang et al. with a threshold current density of $250 \text{ kA}/\text{cm}^2$ (or at least $800 \text{ kW}/\text{cm}^2$ assuming operation at at least 3.2 V) at 386 nm [7] for a $6.5 \mu\text{m}$ thick heterostructure.

It is important to take into account that we are very close to the band gap of GaN (365 nm) in this spectral range (374 - 399 nm). Our waveguides consist to 58% of GaN and to 42% of AlN with 99% of the TE_0 and 94% of the TE_1 modes confined in the GaN layer. Consequently, there is a non-zero absorption loss that needs to be considered. The precise value of below band gap GaN absorption varies from one growth reactor to another but could be in the range of 1000 cm^{-1} at 380 nm [25]. We are thus at the absolute wavelength limit of what can be achieved with a GaN waveguide. In order to descend further in wavelength, we would need to use a waveguide consisting only or mostly of AlN to reduce the absorption loss. Furthermore, using $\text{Al}_x\text{Ga}_{1-x}\text{N}/\text{Al}_y\text{Ga}_{1-y}\text{N}$ ($y > x$) instead of InGaN/GaN

QWs would allow to reduce the emission wavelength into the UV-B and UV-C. Such photonic circuits are feasible, but remain very difficult to implement due to a need for even smaller gaps for efficient coupling as well as difficulties in growing high quality material.

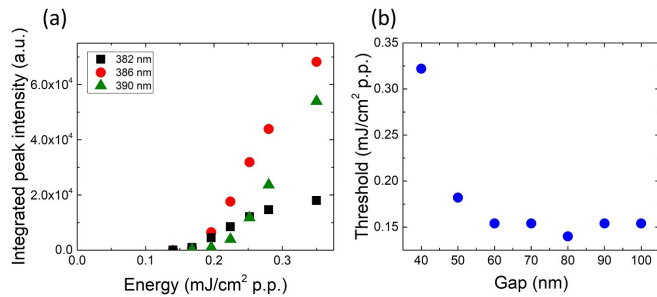


Fig. 4. (a) Integrated peak intensity over pulse energy for the modes at 382, 386, and 390 nm for the device with 90 nm gap shown in Fig. 3 (c,d) and (b) Threshold energy over nominal gap size.

In Fig. 4 (a) we show the integrated peak intensity over the energy per pulse for the modes at 382, 386, and 390 nm, for the device with 90 nm gap (Figs. 3 (c,d)). The lasing thresholds at $E = 0.15$ and 0.19 mJ/cm² per pulse are clearly visible. The threshold energy as a function of nominal gap size is shown in Fig. 4 (b). We can see that the threshold decreases with increasing gap, which is to be expected, since $E_{th} \propto 1/Q_{load}$ and since Q_{load} decreases with increased coupling [16]. For the 40 nm gap, the threshold is particularly high because the gap is not fully open, since these distances are at the limit of what can be achieved using e-beam lithography with UV5 resist.

In conclusion, we have demonstrated active microlaser photonic circuits in the UV-A spectral range using the III-nitride on silicon platform, which is very promising for both active and passive photonic components for next generation photonic integration. Our devices operate at the limit of what can be achieved using GaN as the waveguiding layer. The wavelength can be further reduced by switching from InGaN/GaN to $Al_xGa_{1-x}N/Al_yGa_{1-y}N$ ($y > x$) QWs and the absorption losses can be reduced by using AlN instead of GaN/AlN for the waveguide. Possible applications of such devices could be for gas sensing [26].

We thank Damir Vodenicarevic for his help with python scripts for data analysis. We also thank Sébastien Sauvage for fruitful discussions. This work was supported by the French Agence Nationale de la Recherche (ANR) under MILAGAN convention (ANR-17-CE08-0043-02). We acknowledge support by a public grant overseen by the ANR as part of the “Investissements d’Avenir” program: Labex GANEX (Grant No. ANR-11-LABX-0014). This work was also partly supported by the RENATECH network. We acknowledge the support from the technical teams at PTA-Grenoble, Nanofab (Institut Néel) and CRHEA.

Disclosures. The authors declare no conflicts of interest.

REFERENCES

1. S. Nakamura, *Science* **281**, 956 (1998).
2. M. Kneissl and J. Rass, *III-Nitride Ultraviolet Emitters* (Springer Science & Business Media, 2016).

3. R. Butté and N. Grandjean, *Nanophotonics* **9**, 569 (2020).
4. J. Sellés, C. Brimont, G. Cassabois, P. Valvin, T. Guillet, I. Roland, Y. Zeng, X. Checoury, P. Boucaud, M. Mexis, F. Semond, and B. Gayral, *Sci. Reports* **6**, 21650 (2016).
5. J. Sellés, V. Crepel, I. Roland, M. E. Kurdi, X. Checoury, P. Boucaud, M. Mexis, M. Leroux, B. Damilano, S. Rennesson, F. Semond, B. Gayral, C. Brimont, and T. Guillet, *Appl. Phys. Lett.* **109**, 231101 (2016).
6. G. Zhu, J. Li, N. Zhang, X. Li, J. Dai, Q. Cui, Q. Song, C. Xu, and Y. Wang, *Sci. Reports* **10**, 1 (2020).
7. J. Wang, M. Feng, R. Zhou, Q. Sun, J. Liu, Y. Huang, Y. Zhou, H. Gao, X. Zheng, M. Ikeda, and H. Yang, *Photonics Res.* **7**, B32 (2019).
8. D. J. Blumenthal, *APL Photonics* **5**, 020903 (2020).
9. M. Stegmaier, J. Ebert, J. M. Meckbach, K. Ilin, M. Siegel, and W. H. P. Pernice, *Appl. Phys. Lett.* **104**, 091108 (2014).
10. M. Soltani, R. Soref, T. Palacios, and D. Englund, *Opt. Express* **24**, 25415 (2016).
11. T.-J. Lu, M. Fanto, H. Choi, P. Thomas, J. Steidle, S. Mouradian, W. Kong, D. Zhu, H. Moon, K. Berggren, J. Kim, M. Soltani, S. Preble, and D. Englund, *Opt. Express* **26**, 11147 (2018).
12. X. Liu, A. W. Bruch, Z. Gong, J. Lu, J. B. Surya, L. Zhang, J. Wang, J. Yan, and H. X. Tang, *Optica* **5**, 1279 (2018).
13. G. N. West, W. Loh, D. Kharas, C. Sorace-Asgaskar, K. K. Mehta, J. Sage, J. Chiaverini, and R. J. Ram, *APL Photonics* **4**, 026101 (2019).
14. R. Floyd, K. Hussain, A. Mamun, M. Gaevski, G. Simin, M. Chandrashekhar, and A. Khan, *Appl. Phys. Express* **13**, 022003 (2020).
15. F. Tabataba-Vakili, L. Doyennette, C. Brimont, T. Guillet, S. Rennesson, E. Frayssinet, B. Damilano, J.-Y. Duboz, F. Semond, I. Roland, M. El Kurdi, X. Checoury, S. Sauvage, B. Gayral, and P. Boucaud, *ACS Photonics* **5**, 3643 (2018).
16. F. Tabataba-Vakili, L. Doyennette, C. Brimont, T. Guillet, S. Rennesson, B. Damilano, E. Frayssinet, J.-Y. Duboz, X. Checoury, S. Sauvage, M. El Kurdi, F. Semond, B. Gayral, and P. Boucaud, *Sci Rep* **9**, 18095 (2019).
17. C. H. To, W. Y. Fu, K. H. Li, Y. Cheung, and H. Choi, *Opt. Lett.* **45**, 791 (2020).
18. F. Tabataba-Vakili, S. Rennesson, B. Damilano, E. Frayssinet, J.-Y. Duboz, F. Semond, I. Roland, B. Paulillo, R. Colombelli, M. El Kurdi, X. Checoury, S. Sauvage, L. Doyennette, C. Brimont, T. Guillet, B. Gayral, and P. Boucaud, *Opt. Express* **27**, 11800 (2019).
19. M. Mexis, S. Sergent, T. Guillet, C. Brimont, T. Bretagnon, B. Gil, F. Semond, M. Leroux, D. Néel, S. David, X. Checoury, and P. Boucaud, *Opt. Lett.* **36**, 2203 (2011).
20. I. Rousseau, G. Callsen, G. Jacopin, J.-F. Carlin, R. Butté, and N. Grandjean, *J. Appl. Phys.* **123**, 113103 (2018).
21. L.-W. Luo, G. S. Wiederhecker, J. Cardenas, C. Poitras, and M. Lipson, *Opt. Express* **19**, 6284 (2011).
22. H. A. Haus, M. A. Popović, M. R. Watts, C. Manolatu, B. E. Little, and S. T. Chu, “Optical resonators and filters,” in *Optical microcavities*, (World Scientific, 2004), pp. 1–37.
23. D. Simeonov, E. Feltin, A. Altoukhov, A. Castiglia, J.-F. Carlin, R. Butté, and N. Grandjean, *Appl. Phys. Lett.* **92**, 171102 (2008).
24. E. Young, N. Grandjean, T. Mates, and J. Speck, *Appl. Phys. Lett.* **109**, 212103 (2016).
25. G. Yu, G. Wang, H. Ishikawa, M. Umeno, T. Soga, T. Egawa, J. Watanabe, and T. Jimbo, *Appl. Phys. Lett.* **70**, 3209 (1997).
26. M.-C. Estevez, M. Alvarez, and L. M. Lechuga, *Laser Photonics Rev.* **6**, 463 (2012).

FULL REFERENCES

1. S. Nakamura, "The roles of structural imperfections in InGaN-based blue light-emitting diodes and laser diodes," *Science*, **281**, 956–961 (1998).
2. M. Kneissl and J. Rass, *III-Nitride Ultraviolet Emitters* (Springer Science & Business Media, 2016).
3. R. Butté and N. Grandjean, "III-nitride photonic cavities," *Nanophotonics*, **9**, 569–598 (2020).
4. J. Sellés, C. Brimont, G. Cassabois, P. Valvin, T. Guillet, I. Roland, Y. Zeng, X. Checoury, P. Boucaud, M. Mexis, F. Semond, and B. Gayral, "Deep-UV nitride-on-silicon microdisk lasers," *Sci. Reports* **6**, 21650 (2016).
5. J. Sellés, V. Crepel, I. Roland, M. E. Kurdi, X. Checoury, P. Boucaud, M. Mexis, M. Leroux, B. Damilano, S. Rennesson, F. Semond, B. Gayral, C. Brimont, and T. Guillet, "III-nitride-on-silicon microdisk lasers from the blue to the deep ultra-violet," *Appl. Phys. Lett.* **109**, 231101 (2016).
6. G. Zhu, J. Li, N. Zhang, X. Li, J. Dai, Q. Cui, Q. Song, C. Xu, and Y. Wang, "Whispering-gallery mode lasing in a floating GaN microdisk with a vertical slit," *Sci. Reports* **10**, 1–7 (2020).
7. J. Wang, M. Feng, R. Zhou, Q. Sun, J. Liu, Y. Huang, Y. Zhou, H. Gao, X. Zheng, M. Ikeda, and H. Yang, "GaN-based ultraviolet microdisk laser diode grown on Si," *Photonics Res.* **7**, B32–B35 (2019).
8. D. J. Blumenthal, "Photonic integration for UV to IR applications," *APL Photonics* **5**, 020903 (2020).
9. M. Stegmaier, J. Ebert, J. M. Meckbach, K. Ilin, M. Siegel, and W. H. P. Pernice, "Aluminum nitride nanophotonic circuits operating at ultraviolet wavelengths," *Appl. Phys. Lett.* **104**, 091108 (2014).
10. M. Soltani, R. Soref, T. Palacios, and D. Englund, "AlGaIn/AlN integrated photonics platform for the ultraviolet and visible spectral range," *Opt. Express* **24**, 25415 (2016).
11. T.-J. Lu, M. Fanto, H. Choi, P. Thomas, J. Steidle, S. Mouradian, W. Kong, D. Zhu, H. Moon, K. Berggren, J. Kim, M. Soltani, S. Preble, and D. Englund, "Aluminum nitride integrated photonics platform for the ultraviolet to visible spectrum," *Opt. Express* **26**, 11147–11160 (2018).
12. X. Liu, A. W. Bruch, Z. Gong, J. Lu, J. B. Surya, L. Zhang, J. Wang, J. Yan, and H. X. Tang, "Ultra-high-Q UV microring resonators based on single-crystalline AlN platform," *Optica* **5**, 1279–1282 (2018).
13. G. N. West, W. Loh, D. Kharas, C. Sorace-Agaskar, K. K. Mehta, J. Sage, J. Chiaverini, and R. J. Ram, "Low-loss integrated photonics for the blue and ultraviolet regime," *APL Photonics* **4**, 026101 (2019).
14. R. Floyd, K. Hussain, A. Mamun, M. Gaevski, G. Simin, M. Chandrashekar, and A. Khan, "Photonics integrated circuits using $\text{Al}_x\text{Ga}_{1-x}\text{N}$ based UVC light-emitting diodes, photodetectors and waveguides," *Appl. Phys. Express* **13**, 022003 (2020).
15. F. Tabataba-Vakili, L. Doyennette, C. Brimont, T. Guillet, S. Rennesson, E. Frayssinet, B. Damilano, J.-Y. Duboz, F. Semond, I. Roland, M. El Kurdi, X. Checoury, S. Sauvage, B. Gayral, and P. Boucaud, "Blue microlasers integrated on a photonic platform on silicon," *ACS Photonics* **5**, 3643–3648 (2018).
16. F. Tabataba-Vakili, L. Doyennette, C. Brimont, T. Guillet, S. Rennesson, B. Damilano, E. Frayssinet, J.-Y. Duboz, X. Checoury, S. Sauvage, M. El Kurdi, F. Semond, B. Gayral, and P. Boucaud, "Demonstration of critical coupling in an active III-nitride microdisk photonic circuit on silicon," *Sci Rep* **9**, 18095 (2019).
17. C. H. To, W. Y. Fu, K. H. Li, Y. Cheung, and H. Choi, "GaN microdisk with direct coupled waveguide for unidirectional whispering gallery mode emission," *Opt. Lett.* **45**, 791–794 (2020).
18. F. Tabataba-Vakili, S. Rennesson, B. Damilano, E. Frayssinet, J.-Y. Duboz, F. Semond, I. Roland, B. Paulillo, R. Colombelli, M. El Kurdi, X. Checoury, S. Sauvage, L. Doyennette, C. Brimont, T. Guillet, B. Gayral, and P. Boucaud, "III-nitride on silicon electrically injected microrings for nanophotonic circuits," *Opt. Express* **27**, 11800–11808 (2019).
19. M. Mexis, S. Sergent, T. Guillet, C. Brimont, T. Bretagnon, B. Gil, F. Semond, M. Leroux, D. Néel, S. David, X. Checoury, and P. Boucaud, "High quality factor nitride-based optical cavities: microdisks with embedded GaN/Al(GaN) quantum dots," *Opt. Lett.* **36**, 2203–2205 (2011).
20. I. Rousseau, G. Callsen, G. Jacopin, J.-F. Carlin, R. Butté, and N. Grandjean, "Optical absorption and oxygen passivation of surface states in III-nitride photonic devices," *J. Appl. Phys.* **123**, 113103 (2018).
21. L.-W. Luo, G. S. Wiederhecker, J. Cardenas, C. Poitras, and M. Lipson, "High quality factor etchless silicon photonic ring resonators," *Opt. Express* **19**, 6284–6289 (2011).
22. H. A. Haus, M. A. Popović, M. R. Watts, C. Manolatu, B. E. Little, and S. T. Chu, "Optical resonators and filters," in *Optical microcavities*, (World Scientific, 2004), pp. 1–37.
23. D. Simeonov, E. Feltn, A. Altoukhov, A. Castiglia, J.-F. Carlin, R. Butté, and N. Grandjean, "High quality nitride based microdisks obtained via selective wet etching of AlInN sacrificial layers," *Appl. Phys. Lett.* **92**, 171102 (2008).
24. E. Young, N. Grandjean, T. Mates, and J. Speck, "Calcium impurity as a source of non-radiative recombination in (In, Ga) N layers grown by molecular beam epitaxy," *Appl. Phys. Lett.* **109**, 212103 (2016).
25. G. Yu, G. Wang, H. Ishikawa, M. Umeno, T. Soga, T. Egawa, J. Watanabe, and T. Jimbo, "Optical properties of wurtzite structure GaN on sapphire around fundamental absorption edge (0.78–4.77 eV) by spectroscopic ellipsometry and the optical transmission method," *Appl. Phys. Lett.* **70**, 3209–3211 (1997).
26. M.-C. Estevez, M. Alvarez, and L. M. Lechuga, "Integrated optical devices for lab-on-a-chip biosensing applications," *Laser Photonics Rev.* **6**, 463–487 (2012).